Hindawi
Journal of Energy
Volume 2022, Article ID 7497795, 10 pages
https://doi.org/10.1155/2022/7497795

Research Article

Study of Vertical-Axis Wind Farm Layouts Using a 2D Actuator-Cylinder RANS Model

Edgar Martinez-Ojeda,[1] **Francisco Javier Solorio Ordaz**,[1] **and Mihir Sen**[2]

[1]*Facultad de Ingeniería, Universidad Nacional Autónoma de Mexico, CDMX, México, 04510, Mexico*
[2]*Department of Aerospace and Mechanical Engineering, University of Notre Dame, Notre Dame, IN 46556, USA*

Correspondence should be addressed to Edgar Martinez-Ojeda; eamo87@protonmail.com

Received 10 May 2022; Revised 26 July 2022; Accepted 10 October 2022; Published 21 December 2022

Academic Editor: Viviana C. Mariani

The actuator-cylinder RANS (Reynolds-averaged Navier-Stokes equations) model was used to study the performance of two different arrays of wind turbines. The staggered array proved to be more efficient than the fish-school array (grouped in pairs) in most directions; however, the fish-school array outperformed the conventional staggered array when the pairs of turbines were facing the wind. Increases in global power coefficient up to 16% were found when the wind speed was 8 ms^{-1} and up to 10% when the wind speed was 10 ms^{-1}. Despite the fish-school array being slightly less efficient, this array yielded almost twice as much power density as the staggered array in almost all directions. The current methodology proves to be a fast tool for the estimation of vertical-axis wind turbine farms compared to full RANS simulations.

1. Introduction

Wind farm array modeling in vertical-axis wind turbines (VAWT) is a relatively new field of study. Since large scale experimentation is unlikely, engineers and scientists rely on computer models to analyze the flow around turbines.

The two main methods for studying the flow around turbines are RANS (Reynolds-averaged Navier-Stokes equations) and LES (large eddy simulation) which consist in solving the Navier-Stokes equations; however, a full-rotor simulation is computationally extremely expensive. A virtual method developed by [1] is employed to resolve the flow through the turbine, and it consists in replacing the turbine by volumetric forces dictated by an actuator-cylinder model [2]. This method is able to compute the power coefficient of the turbine as well as resolving the wake.

The main contribution of this work is the usage of the virtual actuator cylinder to provide quick estimates of several wind farm arrays; this is something that has not been done in the past except for a couple of very simple models which are not very accurate. This will also provide insight as to how the wind direction and speed affect the overall performance of the wind farm, which is of utter importance when designing wind farms.

One of the main works done on VAWT farms was by [3], and they used a simple but clever model which constructs the field around a turbine by using superimposed potential flows. Fish-school arrays (pairs of counter-rotating turbines) comprising small wind turbines yielded power density values ranging from 30 up to 100 Wm^{-2}, whereas experimental data from HAWT farms show power densities ranging from 2 up to 6 Wm^{-2} [4]. An experimental study using rather tiny turbines shows that pairs of counter-rotating VAWTs can yield 16% more energy than an isolated VAWT [5]. [6] also found a similar value in the power increase except that he used a RANS simulation by employing large corotating turbines and varying the angle of wind incidence. Another study done using a multiple actuator cylinder shows a power increase up to 5–6% when using pairs of VAWTs rather than isolated turbines [7].

All of the aforementioned studies lack depth when investigating the effect of wind speed and direction, e.g., most of them only use one pair of turbines, fixed velocities, or do not reveal the behavior of the array with respect to the wind

direction. The present study aims to fill those gaps by making use of the virtual actuator cylinder. The other purpose of the study is to analyze the outcomes of two different wind farms, namely, the staggered configuration and the fish-school configuration.

2. RANS-AC Model

The actuator cylinder [2] is a solution of the Euler equations with source terms coming from the volumetric force exerted by the blades of the turbine. The turbine is idealized as a hollow cylinder with finite thickness, and the volumetric forces acting through the thickness of the hollow cylinder create the forces acting on the fluid. The solution for the deficit velocities is shown in Equations (1a) and (1b); i is the current point index, N is the number of evaluation points, θ is the angle of the current evaluation point, and ϕ is a dummy angle used for integration. The normal forces exerted on the cylinder are Q_n.

$$w_x = -\frac{1}{2\pi}\sum_{i=0}^{N-1} Q_{n,i}\int_{\theta_i-(1/2)\Delta\theta}^{\theta_i+(1/2)\Delta\theta} \frac{-(x+\sin\phi)\sin\phi + (y-\cos\phi)\cos\phi}{(x+\sin\phi)^2 + (y-\cos\phi)^2}\, d\phi \underbrace{-Q_n(\arccos y)}_{\text{I}} \underbrace{+\, Q_n(-\arccos y)}_{\text{II}}, \tag{1a}$$

$$w_y = -\frac{1}{2\pi}\sum_{i=0}^{N-1} Q_{n,i}\int_{\theta_i-\left(\frac{1}{2}\right)\Delta\theta}^{\theta_i+\left(\frac{1}{2}\right)\Delta\theta} \frac{-(x+\sin\phi)\cos\phi - (y-\cos\phi)\sin\phi}{(x+\sin\phi)^2 + (y-\cos\phi)^2}\, d\phi. \tag{1b}$$

Since the normal loads are not known beforehand, the AC model draws upon the blade element theory in order to compute the normal loads. The solution is iterative since the normal loads also depend on the velocity deficits, and thus an initial value of zero is prescribed to the velocity deficits, then the loads are computed and so are the velocity deficits. In order to calculate the volumetric force acting on the fluid, it is necessary to remind the definition of the normal loads according to the actuator cylinder theory in Equation (3), where dr is a radial differential, θ is the azimuth angle, ε is the cylinder's thickness, $f_n(\theta)$ is the normal volumetric force, and R is the cylinder's radius. Thorough details on the numerical procedure can be found in [8–11].

$$Q_n(\theta) = \lim_{\varepsilon \longrightarrow 0}\int_{R-\varepsilon}^{R+\varepsilon} f_n(\theta)dr. \tag{2}$$

Given the fact that the volumetric force does not vary significantly across the thickness, it is possible to rewrite Equation (2) as follows.

$$f_n(\theta) = \frac{Q_n(\theta)}{\Delta r}. \tag{3}$$

Using a modified, simpleFoam, OpenFOAM solver [12] for steady and incompressible turbulent flow, the volumetric forces coming from Equation (4) can be incorporated into the computational domain [1]. The modified solver is called actuator-cylinder simpleFoam. It merely assigns cell zones to a turbine, and the velocity field from these cells feed the actuator cylinder. The volumetric forces are calculated and passed to the corresponding cells of the OpenFOAM volumetric field, thus the flow field is slowed down and a wake is created. A k-ε model is used. This turbulence model is best suited for environmental flows [13–15]. Figure 1 shows the actuator-cylinder model cells implemented in OpenFOAM.

3. Verification with AC Model

This section describes the geometrical and operational parameters of the turbine chosen for the wind farm layout study. One of the precautions that must be attended when using the AC model is to keep the turbine's solidity (σ) low. High values will cause the model to give inaccurate predictions. This is due to the fact that adding too many blades or having a large chord-to-radius ratio will introduce severe flow distortions which are not included in the model. The solidity is defined in Equation (5). N_B is the number of blades, c is the blade's chord, and R is the turbine's radius. It can be seen as the total blades' area divided by the turbine's swept area per unit length. A verification with an LES simulation can be found in the appendix.

$$\sigma = \frac{N_B c}{2R}. \tag{4}$$

A turbine from [6] with a low solidity and low chord-to-radius ratio was chosen for the study. This turbine will be used throughout the rest of the work. The characteristics of this turbine are described in Table 1.

3.1. Sensitivity Analysis. The RANS-AC model should be able to predict the power coefficient as close as the standalone AC. It is important to remind that the original AC is based on the Euler equations and no I value is needed as an input parameter (I being the turbulence intensity defined as the ratio of the velocity fluctuations and the mean velocity); therefore, the value of I at the inlet will be taken as 0.10 which is a typical value for offshore sites [16]. The computational domain is two-dimensional and comprises uniform-squared cells; the distance from the center of the turbine to the inlet is 3D (rotor diameters) and so is the distance from the center of the turbine to the sides of the domain. The distance from the turbine's center to the outlet

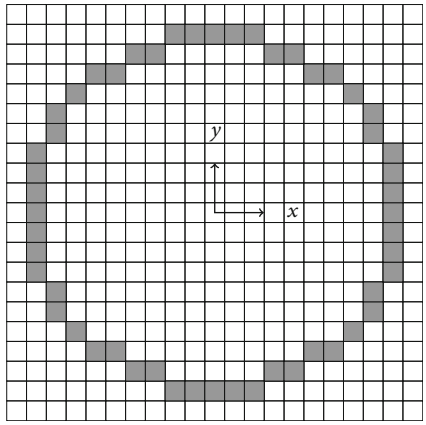

Figure 1: Cells located inside the hollow cylinder. The velocity components of each cell are passed to the stand-alone actuator cylinder model of the actuator cylinder class of the actuator-cylinder simpleFoam solver.

Table 1: Current turbine used throughout this work. N_B is the number of blades, R is the radius, c is the chord, and Ω is the rotational speed in rpm.

Wind turbine characteristics				
NACA	N_B	R	c	Ω
0018	3	10	0.432	33.4

boundary is 10 D. Two meshes were made: a fine one which is based upon a 50×50 cells square surrounding the cylinder and a coarse one which is based upon a 30×30 cells square. The thickness of the actuator is subjective, a value of one chord was chosen for the fine mesh, and a value of two chords was chosen for the coarse mesh. Figure 2 shows the comparison of the power coefficient (C_P) of the RANS-AC model with respect to the stand-alone AC. The tip-speed ratio is the quotient of the turbine's tangential velocity and the wind velocity.

It is believed that the discrepancy in Figure 2 is due to the large distance between the front and rear parts of the actuator cylinder. The AC model assumes that the velocity inside the cylinder is constant streamwise whereas the RANS-AC actually takes into account viscous effects; therefore, the velocity will decay streamwise before impacting the blades in the rear part of the rotor; hence, the lower power coefficients are exhibited by the RANS-AC. Without a validation with an existing turbine, it is hard to know which model yields the best results. The stand-alone AC will surely overestimate the power coefficient in the rear part of the rotor. Verifications and validations of the RANS-AC can be found in [1].

4. Proposed Wind Farm Arrays

In this section, two different kinds of array configurations will be studied, namely, a staggered array and an array based on the fish-schooling concept. According to [3], fish in shoals swim in such a way that each of them sheds counter-rotating vortices which help the shoal to minimize

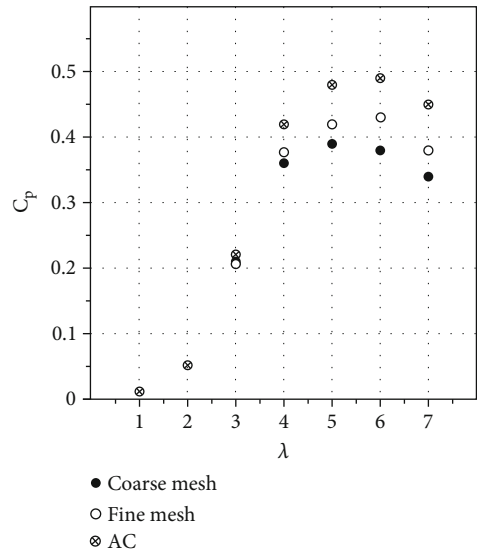

Figure 2: Power coefficients (AC vs RANS-AC) as a function of the tip-speed ratio λ.

the energy needed for propulsion. It is not clear whether the wind farm is the right analogy to fish schools, and little is known as to whether these counter-rotating vortices benefit the turbines in the back rows. The number of turbines is based on the staggered array, then the fish-school array will have twice as many turbines since every turbine in the staggered array will be replaced by a counter-rotating pair of turbines. The reason why the staggered array was chosen is because it is less sensitive to the effect of wind direction provided, and it is aligned with the most frequent sector. Figures 3(a) and 3(b) show the two different arrays that will be studied throughout this work, and the flow is from left to right. The distance from one row to the next nonstaggered row is 8 D; in Figure 3(b), the distance between the axes of each pair is 1.5 D. Before moving on to the details of the simulations, a sensitivity analysis for the mesh size will be carried on. In order to save computational time, it is required to know how close the boundaries can be placed next to the turbines, e.g., placing them too close to the turbines could invalidate the boundary conditions, and placing them too far apart could result in waste of computational time.

4.1. Wind Farm Mesh Sensitivity Analysis. In order to save time during the simulations, four meshes are evaluated. The wind farm tested is that of Figure 3(a). The purpose is to choose the least computationally expensive mesh without losing accuracy. Table 2 shows the characteristics of each mesh.

Figure 4 shows the power coefficients for each mesh. Fine meshes exhibit a slightly larger power coefficient. The back rows are the ones exhibiting more discrepancy, but overall the trend is the same. Figure 5 shows the error between the smallest coarse mesh and the largest fine mesh. The error is about 8% in the turbines that have been blocked by two or more turbines. This is acceptable since the C_P of turbine 16 of the smallest coarse mesh is 0.134, and the C_P of the larges fine mesh is 0.147, compared to the leading turbine's average

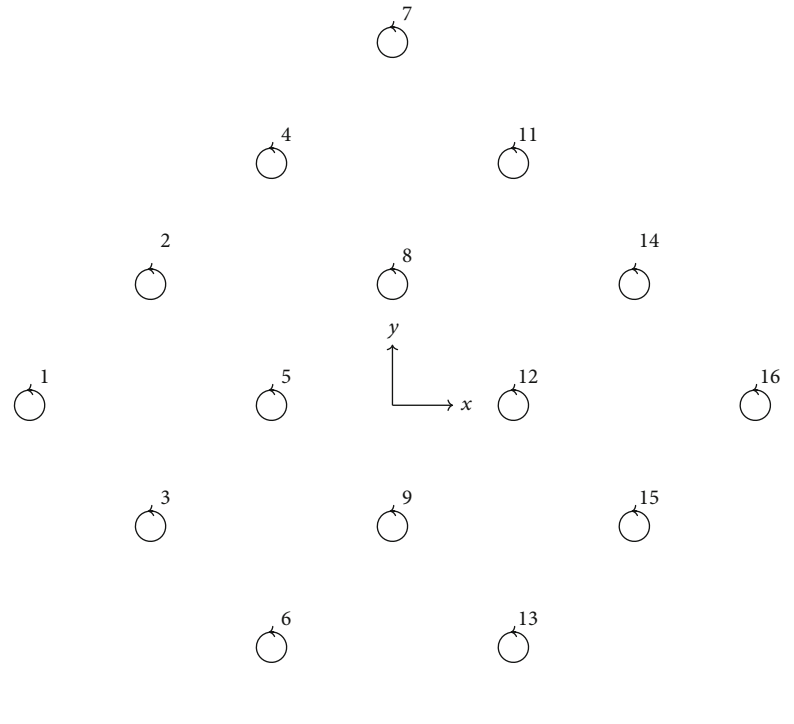

(a) Staggered array

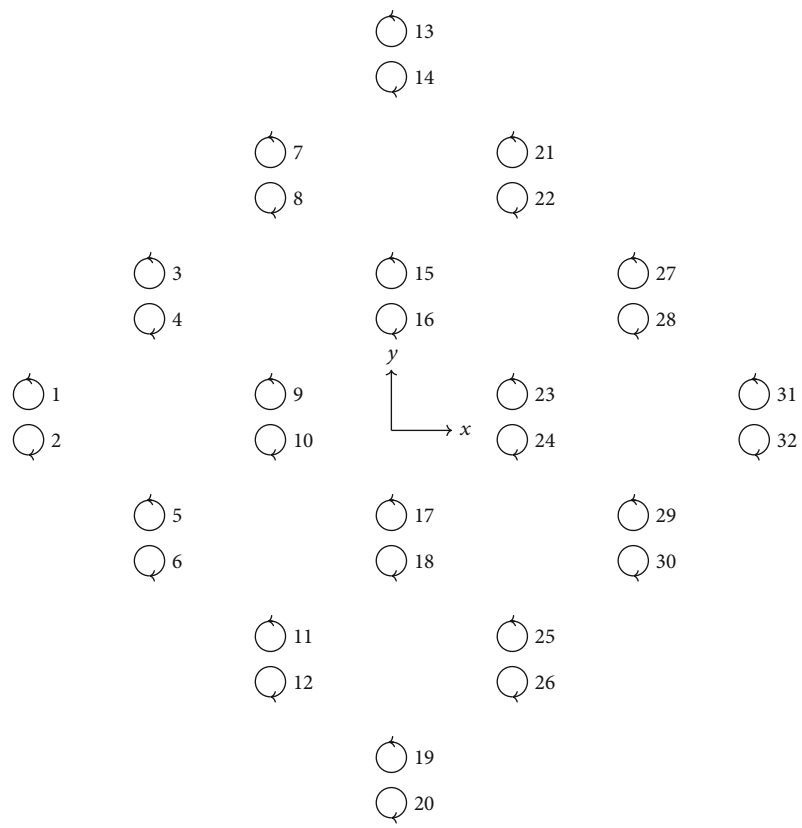

(b) Fisch-school array

Figure 3: The two different arrays that will be used throughout this work. The flow is from left to right.

Table 2: Four kinds of meshes used for the sensitivity study of a wind farm. $\lambda = 4$, $U_\infty = 8.74\,\mathrm{ms}^{-1}$. t is the position of a turbine, e.g., $t_{\min_x}$ is the leftmost turbine's position.

	Tested meshes			
	Square coarse	Rectangular coarse	Square fine	Rectangular fine
Enclosing square size in cells	30×30	30×30	50×50	50×50
$\min_x$	$t_{\min_x} - 6R$	$t_{\min_x} - 6R$	$t_{\min_x} - 6R$	$t_{\min_x} - 6R$
$\max_x$	$t_{\max_x} + 6R$	$t_{\max_x} + 12R$	$t_{\max_x} + 6R$	$t_{\max_x} + 12R$
$\min_y$	$t_{\min_y} - 6R$	$t_{\min_y} - 6R$	$t_{\min_y} - 6R$	$t_{\min_y} - 6R$
$\max_y$	$t_{\max_y} + 6R$	$t_{\max_y} + 6R$	$t_{\max_y} + 6R$	$t_{\max_y} + 6R$
Thickness	$2c$	$2c$	c	c

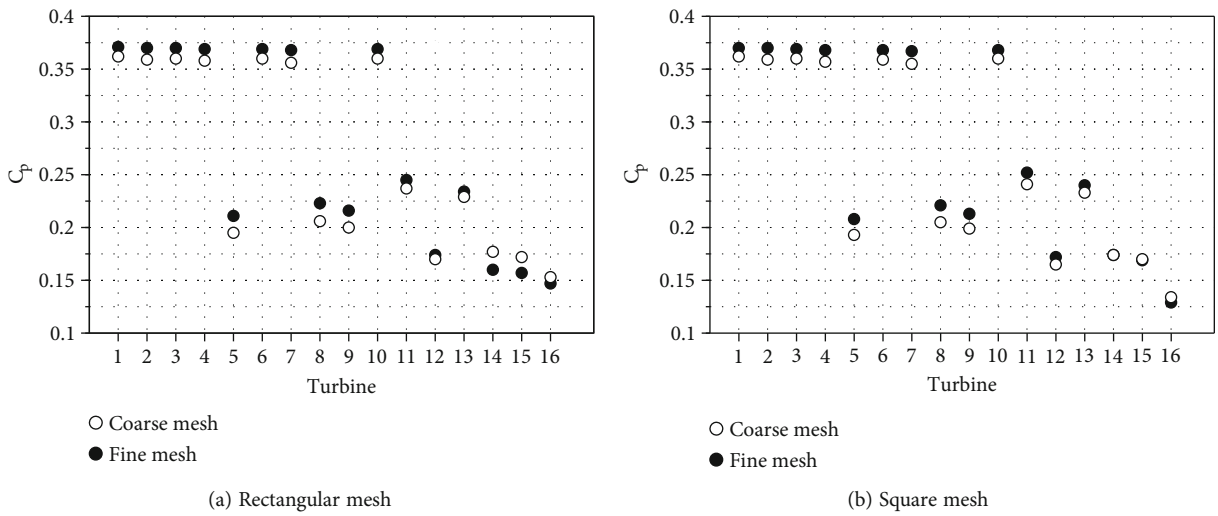

Figure 4: Two different meshes used for sensitivity analysis.

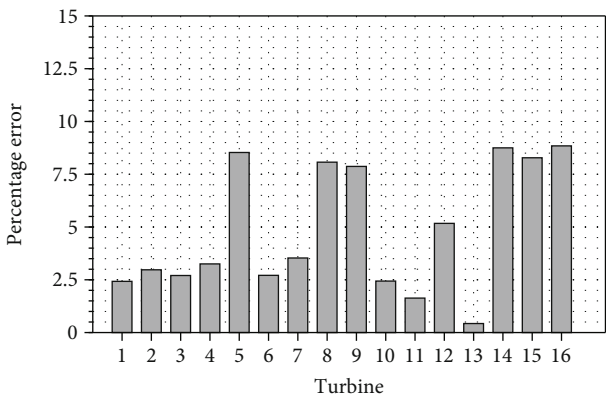

Figure 5: Smallest coarse mesh versus largest fine mesh power coefficient error.

C_P (coarse and fine mesh) which is about 0.366. Their respective normalized C_P is 0.366 and 0.401. In seeing these results, the coarse mesh will be used hereafter.

4.2. Influence of Wind Direction and Wind Speed. Figure 3(a) shows that the wind farm array is symmetrical with respect to the y axis, and this means that it is not necessary to study the full 360° sector but only half of it. Figure 6 shows the nine directions taken into account in this study. Only the most critical wind directions are taken into account. Four different speeds are chosen: 6, 8, 10, and $12\,\mathrm{ms}^{-1}$. The reason is that most wind turbines begin to operate at $5\,\mathrm{ms}^{-1}$, and also, wind speeds higher than $12\,\mathrm{ms}^{-1}$ are rare during the whole year. These considerations will also be applied to the fish-school array.

Turbulence intensity values depend strongly on atmospheric conditions, wind speed, and as well as the roughness of the terrain. A site located in Bockstigen, Sweden will be taken as a reference in order to obtain free stream values of I at different wind speeds. The site is located offshore, and data is provided in [16]. Since the data is a scatter plot from measured values at different speeds, the values in between the minimum and maximum record were chosen from the plot. Table 3 shows the minimum, mean, and maximum values of I for different wind speeds. The height of the mast is 40 m.

Figure 7 shows the average power coefficient of the entire farm as a function of the wind direction and wind speed. The fish-schooling array shows detrimental results when

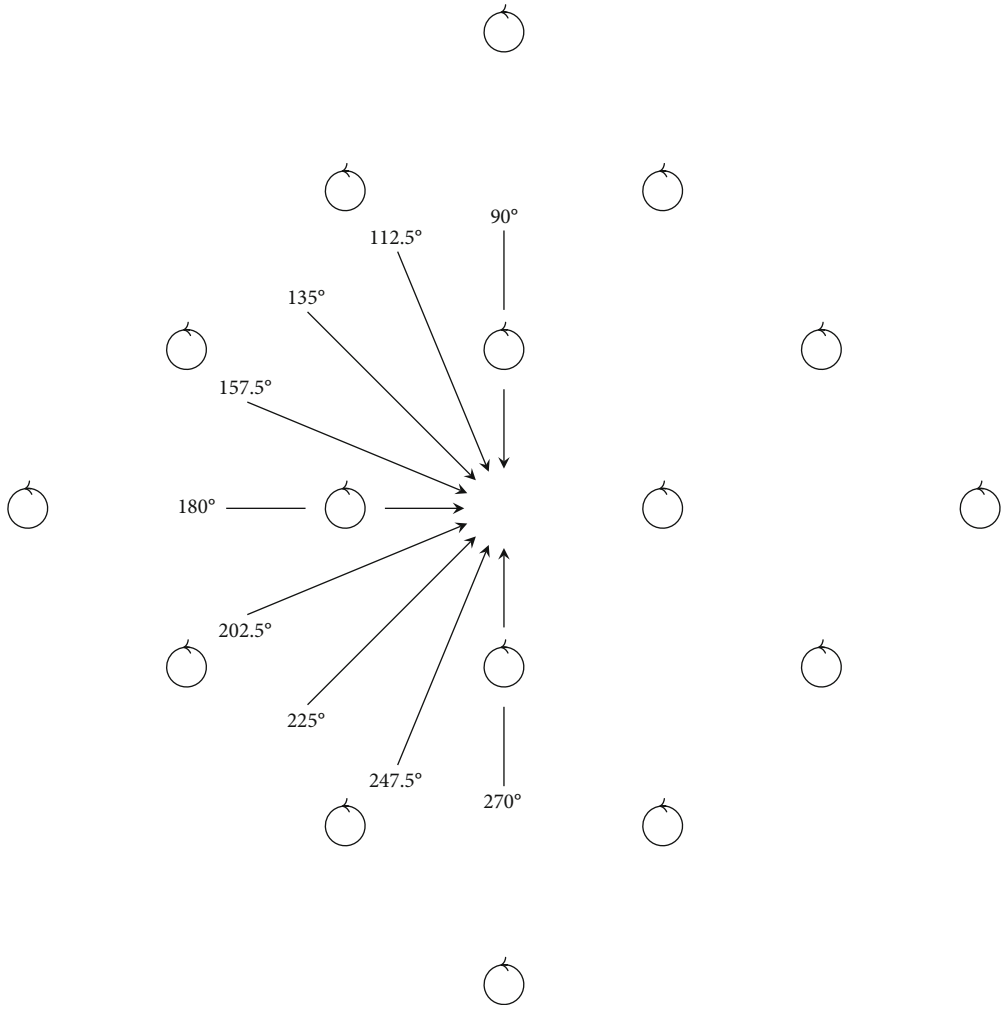

Figure 6: Wind directions that will be used in the current study. Only half the entire sector will be used due to symmetry.

Table 3: Wind data at 40 m from Bockstigen, Gotland, Sweden.

Turbulence intensity according to wind speed					
ms^{-1}	6	8	10	12	14
Min	0.07	0.07	0.075	0.08	0.07
Max	0.25	0.15	0.125	0.12	0.09
Mean	0.16	0.11	0.100	0.10	0.08

the wind blows from the north or the south since half the turbines are blocked by their twins. On the other hand, the fish-schooling array shows an increase of 16% when the wind blows from the west (180°) for the case of $8\,ms^{-1}$, and an increase of 10% is seen for the case of $10\,ms^{-1}$ with wind blowing from the west. This increase in the power coefficient is more or less in accordance to [6], which is 15% roughly for a pair of turbines. Interestingly, at $12\,ms^{-1}$, the average C_P of the farm almost reaches the value of 0.20, which is the C_P of an isolated turbine when $\lambda = 4$, see Figure 2.

Power density is the quotient of the total power produced by the farm divided by the area of land occupied by the turbine; in other words, it is the power extracted by square meter. The surface area of the farm is taken from Figure 3(a). The distance from turbine 1 to turbine 16 is 480 m, therefore the surface area is $115200\,m^2$. In order to calculate the power of a single turbine, it is necessary to know the swept area S which will be taken as $(2R)(2R)$, since $2R$ is the diameter of the turbine. The height of the turbine will be taken as the diameter of the turbine. Equation (5) is necessary to calculate the power of a turbine.

$$P = \frac{1}{2}\rho V_{\infty}^{3} S C_P. \tag{5}$$

The V_{∞} term will be based on the free stream speed for each turbine. Figure 8 shows the power density of the farm as a function of direction and wind speed. This was calculated as the sum of all of the turbines' power divided by the surface area of the farm. The results show a twofold increase in power density in almost all directions for a fish-schooling array, and the only cases where no increase is seen is in the case of $6\,ms^{-1}$ when the wind blows from the north and the south. The almost-twofold increase is expected since there are twice as many turbines

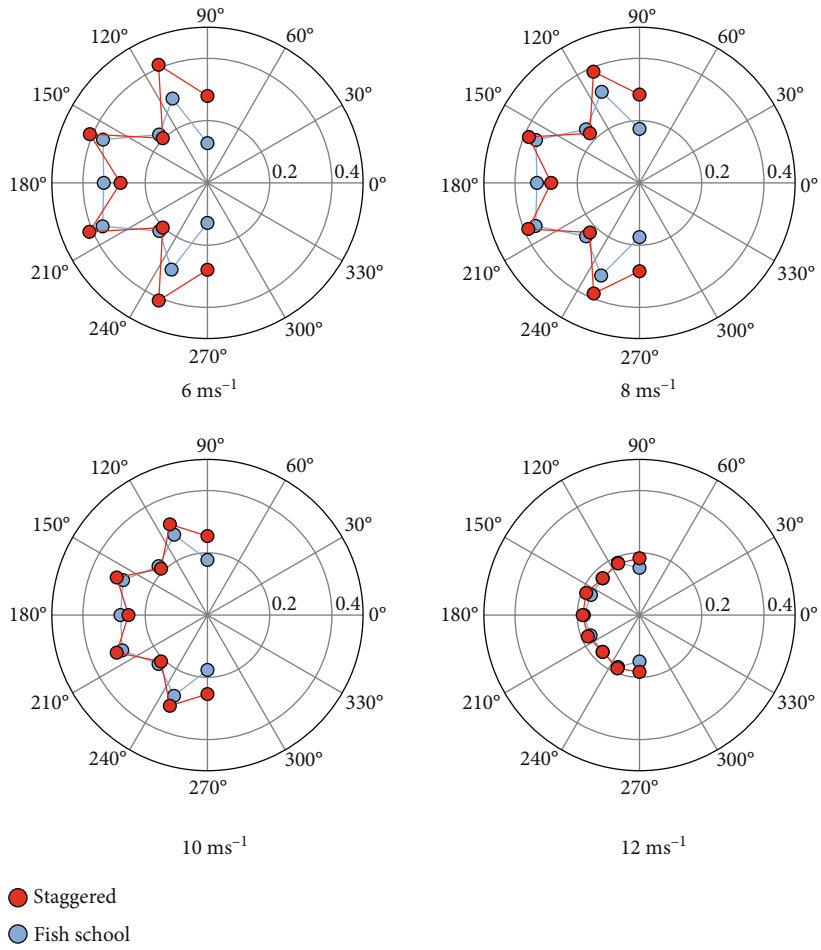

Figure 7: Average power coefficient as a function of direction and wind speed.

in the fish-school farm. There is a dilemma in choosing fish-schooling farms; on the one hand, compactness can yield twice as much power, and on the other hand, these fish-schooling arrays are not necessarily more efficient (Figure 7 shows that the fish-schooling farm is only more efficient than the conventional farms in 3 out of the 9 directions). The bottom line is that one may be able to pack twice as many turbine without losing considerable efficiency. This may vary with the direction of the wind; however, a proper location of the wind farm could result in avoiding the least favorable alignments, for instance, to avoid having the most frequent direction aligned with the local north-to-south axis of the farm (when half the turbines are blocked by their twins).

According to [4], HAWT farms produce around 2–3 Wm^{-2}. Table 4 shows the fish-school and conventional farm average power density (from all directions) for each wind speed. Notice that in actuality, the wind does not blow with the same probability from all directions; therefore, cases in which half the turbines are blocked in the fish-school array (north and south) must be avoided by placing the turbines strategically. It is also worth noticing that in Table 5, the number of power density maxima increases as the wind speed increases too. This may mean that the wind direction is less relevant at higher speeds. The fact of getting almost twice as much power density from the same occupied land can reduce costs dramatically since cabling costs and land rental would probably be half the original cost.

5. Discussion

The RANS actuator cylinder was used to assess the performance of two different wind turbine arrays, namely, a staggered array and another staggered array using pairs of counter-rotating turbines. The power coefficient of a single isolated turbine was tested against the stand-alone AC, and the results were satisfactory except at high tip-speed ratios where the velocity of the wind speed is low. This does not suggest that the RANS-AC is wrong, but its C_P at low wind speeds simply differed from the stand-alone AC because the RANS-AC does indeed take into account viscous effects; therefore, the wind speed impacting the rear part of the rotor is lower than that of the stand-alone AC due to the large distance (20 m maximum, which is the turbine's diameter) from the upwind part of the rotor to the downwind part of the rotor.

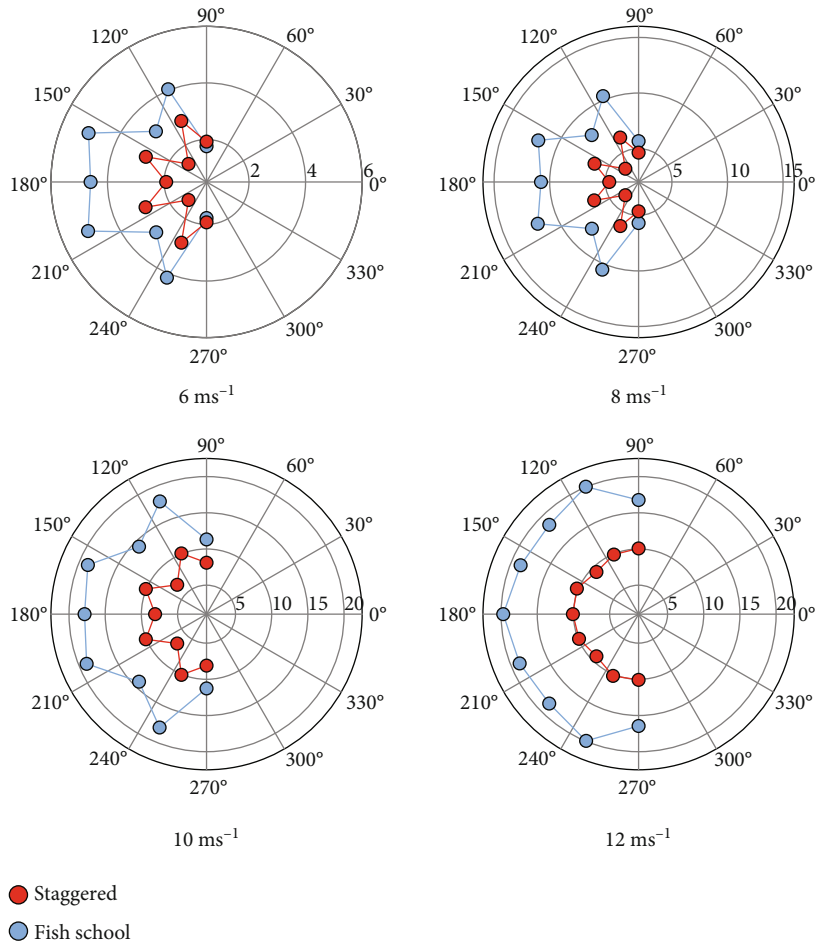

Figure 8: Wind farm power density Wm^{-2} as a function of direction and wind speed.

Table 4: Average power density from all directions.

	Average power density (Wm^{-2})		
ms^{-1}	Fish school	Conventional	Improvement ratio
6	3.8	2.2	1.72
8	9.6	5.2	1.85
10	16.4	8.7	1.88
12	18.8	9.9	1.9

Table 5: Number of occurrences of power density maxima.

	Number of occurrences of power density maxima	
ms^{-1}	Fish school	Conventional
6	1	4
8	1	4
10	2	4
12	3	5

A mesh sensitivity analysis was carried on for a wind farm in order to use the less time-consuming mesh without sacrificing accuracy. The study was undertaken, and several simulations at different wind speeds and directions were done. A coarse mesh was found to be best for the study since it provides accurate result while saving computational time. The value of turbulence intensity at the inlet was chosen based on data acquired from an offshore site off the coast of Sweden.

The staggered array outperformed the fish-school array in most directions, but the fish-school array yielded higher global power coefficients when the wind blows from the west (the case in which all pairs are facing the wind). Improvements up to 16% percent were seen depending on the wind speed. By contrast, the fish-school array outperformed the staggered array by a factor of two in terms of power density. Given the fact that typical HAWT farms yield around 2–3 Wm^{-2}, it can be said that VAWT farms yield in this case 5 or 3 times more power density when the wind blows at 8 ms^{-1}. The fish-school array power density averaged over all directions was practically twice as high as in the staggered array. This proves that the fish-school array may be able to extract twice as much energy so long it is placed strategically. VAWT farms could be compacted within a surface area half the original size and still get almost twice as much power density. This could reduce land costs as well as cabling significantly.

Aided by recent improvements in materials and bearing technology, these fish-school arrays have the potential of extracting more power per unit area as compared to HAWT

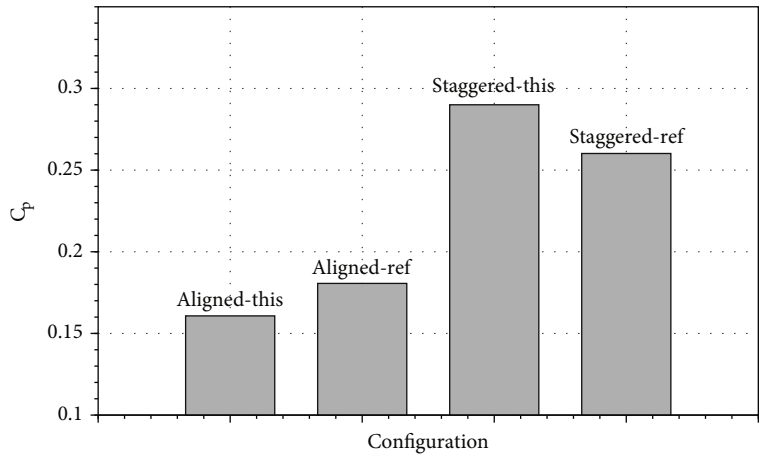

Figure 9: Average C_P comparisons of aligned and staggered wind farms.

farms; however, there is a trade-off: they can be a little less inefficient, especially when half the twin turbines are blocked. Another matter in consideration is that little is known about how the turbulence created by these turbines will affect the turbines further back, e.g., whereas placing them too close can increase the power coefficient, it could also damage them by creating vibrations on the structure. Further investigation on wake turbulence effects on other turbines is needed to approve the fish-school arrays.

Appendix

Verification against an LES Simulation

A simulation done against wind farm LES results from [17] is included as a verification of the model. These results reveal the behavior of two different wind farms: a formation with aligned turbines and staggered rows. The turbine was a Windspire of 1.2 m in diameter, full specifications are describe in [17]. Both wind farms contained 32 turbines, that is 8 rows containing 4 turbines; the distance between turbines was 10 D.

Finally, Figure 9 shows the average power coefficient of each wind farm. Overall there is good agreement; however, the current model underpredicts in the aligned formations and it overpredicts in the staggered formation. It was expected to have a higher power coefficient for the staggered formatio n since there is less blockage in the first rows. It is important to mention that there is not too much information in the literature to validate with, as VAWT farms are practically inexistent at the moment. Most data from VAWT farms comes from simulations, and on top of that, most researchers choose small wind turbines (large solidity) which makes it even more difficult for this model to find appropriate conditions for a thorough verification. It is hoped that more studies arise in the years to come.

Data Availability

Code in OpenFOAM can be found at doi:10.5281/zenodo .5177216. Data can be found in doi:10.5281/zenodo.6463998.

Conflicts of Interest

The authors declare that they have no conflict of interest.

Authors' Contributions

Edgar Martinez-Ojeda was the main contributor, Francisco Javier and Mihir aided in the writing process.

Acknowledgments

The first author of this work would like to thank CONACYT (Consejo Nacional de Ciencia y Tecnología) as well as the OpenFOAM community.

References

[1] E. Martinez-Ojeda, F. J. S. Ordaz, and M. Sen, "Vertical-axis wind-turbine computations using a 2D hybrid wake actuator-cylinder model," *Wind Energy Science*, vol. 6, no. 4, pp. 1061–1077, 2021.

[2] H. Madsen, *The Actuator Cylinder: A Flow Model for Vertical-Axis Wind Turbines, [Ph.D. thesis]*, Aalborg University Centre, 1982.

[3] R. W. Whittlesey, S. Liska, and J. Dabiri, "fish schooling as a basis for vertical axis wind turbine farm design," *Bioinspiration & Biomimetics*, vol. 5, no. 3, p. 035005, 2010.

[4] J. O. Dabiri, "Potential order-of-magnitude enhancement of wind farm power density via counter-rotating vertical-axis wind turbine arrays," *Journal of Renewable and Sustainable Energy*, vol. 3, no. 4, 2011.

[5] A. Vergaerde, T. D. Troyer, S. Muggiasca, I. Bayati, M. Belloli, and M. Runacres, "influence of the direction of rotation on the wake characteristics of closely spaced counter-rotating vertical-axis wind turbines," *Journal of Physics: Conference Series*, vol. 1618, no. 6, article 062017, 2020.

[6] J. T. Hansen, M. Mahak, and I. Tzanakis, "Numerical modelling and optimization of vertical axis wind turbine pairs: a scale up approach," *Renewable Energy*, vol. 171, pp. 1371–1381, 2021.

[7] C. Shovanec and R. Argawal, *K.: CFD Study of Wake Interactions from Multiple Vertical Axis Wind Turbines Using Actuator Cylinder Theory, Mechanical Engineering and Materials*

Science Independent Study, Washington University, St. Louis, MO, USA, 2020.

[8] Z. Cheng, H. A. Madsen, Z. Gao, and T. Moan, "Aerodynamic modeling of floating vertical Axis wind turbines using the actuator cylinder flow method," *Energy Procedia*, vol. 94, pp. 531–543, 2016.

[9] A. Li, *Double Actuator Cylinder Model of a Tandem Vertical-Axis Wind Turbine Counter-Rotating Rotor Concept Operating in Different Wind Conditions, [M.S. thesis]*, Technical University of Denmark, 2017.

[10] H. Madsen, T. Larsen, L. Vita, and U. Paulsen, "Implementation of the actuator cylinder flow model in the hawc2 code for aeroelastic simulations on vertical axis wind turbines," *51st AIAA Aerospace Sciences Meeting including the New Horizons Forum and Aerospace Exposition*, 2013, Grapevine, TX, USA, 2013.

[11] A. Ning, "Actuator cylinder theory for multiple vertical axis wind turbines," *Wind Energy Science*, vol. 1, no. 2, pp. 327–340, 2016.

[12] F. Moukalled, L. Mangani, and M. Darwish, *The Finite Volume Method in Computational Fluid Dynamics an Advanced Introduction with OpenFOAM and Matlab*, Springer, 1st edition, 2016.

[13] J. Bardina, P. Huang, and T. Coakley, *Turbulence modeling validation, testing, and development*, Tech. Rep., 1997.

[14] B. Launder and D. Spalding, "The numerical computation of turbulent flows," *Applied Mechanics and Engineering*, vol. 3, no. 2, pp. 269–289, 1974.

[15] D. Wilcox, *Turbulence Modeling for CFD*, DCW Industries, Anaheim, CA, USA, 2nd edition, 1998.

[16] G. Larsen and K. Hansen, "Database on Wind characteristics, contents of database bank, revision I," Tech. Rep., Riso National Laboratory, Roskilde, Denmark, 2004.

[17] S. Hezaveh, E. Bou-Zeid, J. Dabiri, M. Kinzel, G. Cortina, and L. Martinelli, "Increasing the power production of vertical-Axis wind-turbine farms using synergistic clustering," *Boundary-Layer Meteorology*, vol. 169, no. 2, pp. 275–296, 2018.